Edge-reflection phase directed plasmonic resonances on graphene nano-structures

Luping Du,[1] Dingyuan Tang,[1,*] and Xiaocong Yuan[2,3]

[1]*School of Electrical & Electronic Engineering, Nanyang Technological University, 50 Nanyang Avenue, 639798, Singapore*

[2]*Institute of Micro & Nano Optics, Key Laboratory of Optoelectronic Devices and Systems of Ministry of Education and Guangdong Province, College of Optoelectronic Engineering, Shenzhen University, Shenzhen, 518060, China*

[3]*xcyuan@szu.edu.cn*

**edytang@ntu.edu.sg*

Abstract: The phase of graphene plasmon upon edge-reflection plays a crucial role on determining the spectral properties of graphene structures. In this article, by using the full-wave simulation, we demonstrate that the mid-infrared graphene plasmons are nearly totally reflected at the boundary together with a phase jump of approximately 0.27π, regardless of the environments surrounding it. Appling this phase pickup, a Fabry-Perot model is formulated that can predict accurately the resonant wavelengths of graphene nano-ribbons. Furthermore, we find that the magnitude of the phase jump will either increase or reduce when two neighboring coplanar graphene sheets couple with each other. This could be used to explain the red-shift of resonant wavelength of periodic ribbon arrays with respect to an isolated ribbon. We provide a straightforward way to uncover the phase jump of graphene plasmons that would be helpful for designing and engineering graphene resonators and waveguides as well as their associated applications.

OCIS codes: (160.4670) Optical materials; (240.6680) Surface plasmons; (350.5030) Phase; (120.2230) Fabry-Perot; (260.5740) Resonance.

References and links:

1. W. L. Barnes, A. Dereux, and T. W. Ebbesen, "Surface plasmon subwavelength optics," Nature **424**(6950), 824–830 (2003).
2. E. Hao and G. C. Schatz, "Electromagnetic fields around silver nanoparticles and dimers," J. Chem. Phys. **120**(1), 357–366 (2004).
3. J. Homola, S. S. Yee, and G. Gauglitz, "Surface plasmon resonance sensors: review," Sens. Actuators B Chem. **54**(1-2), 3–15 (1999).
4. R. Wang, L. Du, C. Zhang, Z. Man, Y. Wang, S. Wei, C. Min, S. Zhu, and X. C. Yuan, "Plasmonic petal-shaped beam for microscopic phase-sensitive SPR biosensor with ultrahigh sensitivity," Opt. Lett. **38**(22), 4770–4773 (2013).
5. J. B. Pendry, "Negative refraction makes a perfect lens," Phys. Rev. Lett. **85**(18), 3966–3969 (2000).
6. N. Fang, H. Lee, C. Sun, and X. Zhang, "Sub-diffraction-limited optical imaging with a silver superlens," Science **308**(5721), 534–537 (2005).
7. S. M. Nie and S. R. Emory, "Probing single molecules and single nanoparticles by surface-enhanced Raman scattering," Science **275**(5303), 1102–1106 (1997).
8. K. Kneipp, Y. Wang, H. Kneipp, L. T. Perelman, I. Itzkan, R. Dasari, and M. S. Feld, "Single molecule detection using surface-enhanced Raman scattering (SERS)," Phys. Rev. Lett. **78**(9), 1667–1670 (1997).
9. L. P. Du, G. H. Yuan, D. Y. Tang, and X. C. Yuan, "Tightly focused radially polarized beam for propagating surface plasmon-assisted gap-mode Raman spectroscopy," Plasmonics **6**(4), 651–657 (2011).
10. V. J. Sorger, R. F. Oulton, R. M. Ma, and X. Zhang, "Toward integrated plasmonic circuits," MRS Bull. **37**(08), 728–738 (2012).
11. A. K. Geim and K. S. Novoselov, "The rise of graphene," Nat. Mater. **6**(3), 183–191 (2007).
12. K. S. Novoselov, V. I. Fal'ko, L. Colombo, P. R. Gellert, M. G. Schwab, and K. Kim, "A roadmap for graphene," Nature **490**(7419), 192–200 (2012).
13. A. N. Grigorenko, M. Polini, and K. S. Novoselov, "Graphene plasmonics," Nat. Photonics **6**(11), 749–758 (2012).

#217429 - $15.00 USD Received 21 Jul 2014; revised 17 Aug 2014; accepted 23 Aug 2014; published 11 Sep 2014

14. Q. L. Bao and K. P. Loh, "Graphene photonics, plasmonics, and broadband optoelectronic devices," ACS Nano **6**(5), 3677–3694 (2012).
15. H. X. Da, Q. L. Bao, R. Sanaei, J. H. Teng, K. P. Loh, F. J. Garcia-Vidal, and C. W. Qiu, "Monolayer graphene photonic metastructures: giant Faraday rotation and nearly perfect transmission," Phys. Rev. B **88**(20), 205405 (2013).
16. M. Jablan, H. Buljan, and M. Soljacic, "Plasmonics in graphene at infrared frequencies," Phys. Rev. B **80**(24), 245435 (2009).
17. L. Ju, B. S. Geng, J. Horng, C. Girit, M. Martin, Z. Hao, H. A. Bechtel, X. G. Liang, A. Zettl, Y. R. Shen, and F. Wang, "Graphene plasmonics for tunable terahertz metamaterials," Nat. Nanotechnol. **6**(10), 630–634 (2011).
18. H. Yan, X. Li, B. Chandra, G. Tulevski, Y. Wu, M. Freitag, W. Zhu, P. Avouris, and F. Xia, "Tunable infrared plasmonic devices using graphene/insulator stacks," Nat. Nanotechnol. **7**(5), 330–334 (2012).
19. H. G. Yan, T. Low, W. J. Zhu, Y. Q. Wu, M. Freitag, X. S. Li, F. Guinea, P. Avouris, and F. N. Xia, "Damping pathways of mid-infrared plasmons in graphene nanostructures," Nat. Photonics **7**(5), 394–399 (2013).
20. J. N. Chen, M. Badioli, P. Alonso-González, S. Thongrattanasiri, F. Huth, J. Osmond, M. Spasenović, A. Centeno, A. Pesquera, P. Godignon, A. Z. Elorza, N. Camara, F. J. García de Abajo, R. Hillenbrand, and F. H. L. Koppens, "Optical nano-imaging of gate-tunable graphene plasmons," Nature **487**(7405), 77–81 (2012).
21. Z. Fei, A. S. Rodin, G. O. Andreev, W. Bao, A. S. McLeod, M. Wagner, L. M. Zhang, Z. Zhao, M. Thiemens, G. Dominguez, M. M. Fogler, A. H. Castro Neto, C. N. Lau, F. Keilmann, and D. N. Basov, "Gate-tuning of graphene plasmons revealed by infrared nano-imaging," Nature **487**(7405), 82–85 (2012).
22. F. H. L. Koppens, D. E. Chang, and F. J. García de Abajo, "Graphene plasmonics: a platform for strong light-matter interactions," Nano Lett. **11**(8), 3370–3377 (2011).
23. J. Christensen, A. Manjavacas, S. Thongrattanasiri, F. H. L. Koppens, and F. J. de Abajo, "Graphene plasmon waveguiding and hybridization in individual and paired nanoribbons," ACS Nano **6**(1), 431–440 (2012).
24. J. T. Kim and S. Y. Choi, "Graphene-based plasmonic waveguides for photonic integrated circuits," Opt. Express **19**(24), 24557–24562 (2011).
25. A. Y. Nikitin, F. Guinea, F. J. García-Vidal, and L. Martín-Moreno, "Edge and waveguide terahertz surface plasmon modes in graphene microribbons," Phys. Rev. B **84**(16), 161407 (2011).
26. B. Wang, X. Zhang, F. J. García-Vidal, X. C. Yuan, and J. Teng, "Strong coupling of surface plasmon polaritons in monolayer graphene sheet arrays," Phys. Rev. Lett. **109**(7), 073901 (2012).
27. B. Wang, X. Zhang, X. C. Yuan, and J. H. Teng, "Optical coupling of surface plasmons between graphene sheets," Appl. Phys. Lett. **100**(13), 131111 (2012).
28. V. W. Brar, M. S. Jang, M. Sherrott, J. J. Lopez, and H. A. Atwater, "Highly confined tunable mid-infrared plasmonics in graphene nanoresonators," Nano Lett. **13**(6), 2541–2547 (2013).
29. H. Ju Xu, W. Bing Lu, W. Zhu, Z. Gao Dong, and T. Jun Cui, "Efficient manipulation of surface plasmon polariton waves in graphene," Appl. Phys. Lett. **100**(24), 243110 (2012).
30. L. Wang, W. Cai, X. Z. Zhang, P. H. Liu, Y. X. Xiang, and J. J. Xu, "Mid-infrared optical near-field switching in heterogeneous graphene ribbon pairs," Appl. Phys. Lett. **103**(4), 041604 (2013).
31. X. L. Zhu, W. Yan, N. A. Mortensen, and S. S. Xiao, "Bends and splitters in graphene nanoribbon waveguides," Opt. Express **21**(3), 3486–3491 (2013).
32. L. Du and D. Tang, "Manipulating propagating graphene plasmons at near field by shaped graphene nano-vacancies," J. Opt. Soc. Am. A **31**(4), 691–695 (2014).
33. J. H. Strait, P. Nene, W. M. Chan, C. Manolatou, S. Tiwari, F. Rana, J. W. Kevek, and P. L. McEuen, "Confined plasmons in graphene microstructures: experiments and theory," Phys. Rev. B **87**(24), 241410 (2013).
34. J. Dorfmüller, R. Vogelgesang, R. T. Weitz, C. Rockstuhl, C. Etrich, T. Pertsch, F. Lederer, and K. Kern, "Fabry-Pérot resonances in one-dimensional plasmonic nanostructures," Nano Lett. **9**(6), 2372–2377 (2009).
35. E. S. Barnard, J. S. White, A. Chandran, and M. L. Brongersma, "Spectral properties of plasmonic resonator antennas," Opt. Express **16**(21), 16529–16537 (2008).
36. G. Della Valle, T. Sondergaard, and S. I. Bozhevolnyi, "Plasmon-polariton nano-strip resonators: from visible to infra-red," Opt. Express **16**(10), 6867–6876 (2008).
37. T. Søndergaard, J. Beermann, A. Boltasseva, and S. I. Bozhevolnyi, "Slow-plasmon resonant-nanostrip antennas: analysis and demonstration," Phys. Rev. B **77**(11), 115420 (2008).
38. R. Gordon, "Light in a subwavelength slit in a metal: propagation and reflection," Phys. Rev. B **73**(15), 153405 (2006).
39. A. Chandran, E. S. Barnard, J. S. White, and M. L. Brongersma, "Metal-dielectric-metal surface plasmon-polariton resonators," Phys. Rev. B **85**(8), 085416 (2012).
40. F. J. G. de Abajo, "Graphene plasmonics: challenges and opportunities," Acs Photonics **1**(3), 135–152 (2014).
41. M. Jablan, M. Soljacic, and H. Buljan, "Plasmons in graphene: fundamental properties and potential applications," Proc. IEEE **101**(7), 1689–1704 (2013).
42. S. E. Kocabaş, G. Veronis, D. A. B. Miller, and S. H. Fan, "Modal analysis and coupling in metal-insulator-metal waveguides," Phys. Rev. B **79**(3), 035120 (2009).
43. M. G. Moharam, E. B. Grann, D. A. Pommet, and T. K. Gaylord, "Formulation for stable and efficient implementation of the rigorous coupled-wave analysis of binary gratings," J. Opt. Soc. Am. A **12**(5), 1068–1076 (1995).

#217429 - $15.00 USD Received 21 Jul 2014; revised 17 Aug 2014; accepted 23 Aug 2014; published 11 Sep 2014

1. Introduction

When a light illuminates on to a smooth conductor surface or nano-structures, the collective oscillation of free electrons with incident radiation is possible under certain conditions, generating the so-called surface plasmons (SPs) [1]. Under this circumstance, the electromagnetic field is strongly confined at the surface of nano-structures together with a large field enhancement [2]. These unique properties associated with SPs host a variety of applications ranging from bio-sensing [3, 4], imaging [5, 6], and Raman spectroscopy [7–9] to the miniaturization of nanophotonics circuits [10].

As an alternative plasmonic material, graphene [11, 12], an atomic layer of carbon, has drawn great amount of interests recently in nanophotonics [13–15]. It was predicted that a highly-doped graphene is able to support SPs at mid-infrared frequencies with much higher degree of spatial confinement and relatively lower losses with respect to the noble metal plasmons, and more notably, with tunability either by chemical or electrical doping [16]. They were subsequently uncovered experimentally at graphene micro-and nano-structures [17–19] (ribbon, disk, etc.) and most recently at extended graphene sheets [20,21], rendering graphene plasmons rapidly emerging as a powerful tool for tunable light control at deep-subwavelength scale [22–33].

The spectral properties of graphene structures depend strongly on the feature size of the structure as well as the material properties of graphene such as Fermi energy and mobility. For a ribbon structure, a scaling law is formulated by using the quasi-static analysis bridging the plasmon frequencies with the geometric and material parameters of graphene [17, 23]. However, the quasi-static analysis could not bring a clear physical interpretation to the resonance and is indeed not able to predict the peak wavelengths of a give ribbon. The Fabry-Perot (F-P) model could potentially interpret the resonance of graphene structures, which is prevailing in noble metal plasmons to describe the localized plasmons on nano-wires [34], nano-stripes [35–37] and truncated metal-dielectric-metal waveguides [38, 39]. The SPs supported on the nano-structures undergo multiple reflections from the end-terminations and a resonance occurs once the round-trip phase equals to $m \cdot 2\pi$ (m is an integer), which gives rise to a constructive interference between the forward and back-forward SPs. The same circumstance also applies to the wave-guiding plasmons propagating along graphene ribbons [40]. In that case, the electromagnetic field at the lateral direction (i.e., across the ribbon) should form a standing wave to give rise to a guided plasmon mode. Thus, the phase associated with each reflection becomes critical in order to provide an accurate prediction of the F-P resonances of nano-structures and the dispersion relation of the wave-guiding modes. In recent years, a few studies have engaged in obtaining the reflection phase of noble metal plasmons, including the direct analytical calculation [38], the numerical simulation with finite-difference frequency-domain method [35] and some indirect approaches by fitting the resonances with F-P model [36, 37].

In this work, we study for the first time the phase of SPs upon reflection at the boundary of graphene, which is extracted from the interference fringes between the forward and reflected SPs. An analytical estimation of the reflection coefficient is also present to study its spectral responses. The F-P model is then formulated to predict the resonance frequencies of an isolated graphene ribbon. Furthermore, using the same approach, the phase jump in the case of a pair of neighboring coplanar graphene sheets is investigated. The magnitude of phase pickup either increases or decreases depending on the coupling scheme between the two graphene sheets, which could potentially be used for explaining the red-shift of resonance wavelength of periodic ribbon arrays and the energy splitting of the wave-guiding plasmons at a pair of neighboring coplanar graphene ribbons.

#217429 - $15.00 USD Received 21 Jul 2014; revised 17 Aug 2014; accepted 23 Aug 2014; published 11 Sep 2014

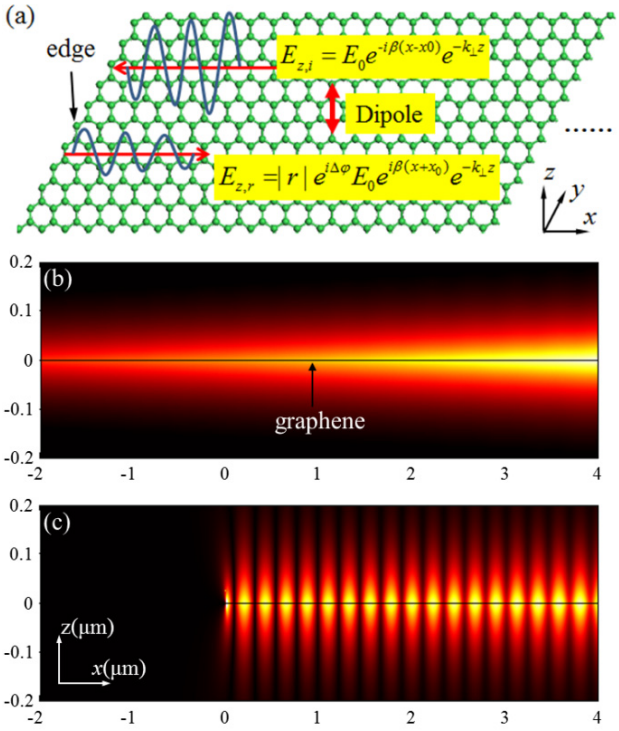

Fig. 1. (a) Schematic diagram illustrating the edge reflection of graphene surface plasmon, assuming a reflection co-efficient of $|r|\cdot\exp(i\Delta\varphi)$. (b) and (c) $|E_z|$ distributions in the vicinity of graphene without and with a boundary. The presence of a boundary will give rise to a self-interference pattern, with the positions of the fringes solely determined by the reflection phase of graphene plasmon. In the simulation, the refractive indices above and below graphene are set to be 1 and 1.5, respectively.

2. Reflection coefficients of graphene surface plasmons.

Surface plasmon at graphene can be considered as a TM polarized odd coupling mode of an insulator-conductor-insulator heterostructure [41]. Its dispersion relation could be obtained in the $d\rightarrow 0$ limit (where d is the thickness of the conductor film), which can mathematically be expressed as:

$$\beta = \frac{\varepsilon_0(\varepsilon_1+\varepsilon_2)}{2}\cdot\frac{2i\omega_0}{\sigma_g} \tag{1}$$

In the formula, β denotes the wave-vector of SPs, ε_1 and ε_2 the permittivities of the mediums above and below graphene, σ_g the conductivity of graphene and ω_0 the incident frequency, respectively. Considering a line dipole source located at $x = x_0$ right above graphene [Fig. 1(a)], it is able to launch SPs at graphene, which have well- defined z-component electric field expressed as $\boldsymbol{E}_z = \boldsymbol{E_0}\cdot\exp(-i\beta(x-x_0))\cdot\exp(-k_\perp z)$, in which $k_\perp = (\beta^2-k_0^2)^{1/2}$ represents the perpendicular wave-vector component of graphene plasmon.

Figure 1(b) and 1(c) show the distribution of the z-component electric field in the vicinity of graphene obtained with FDTD method at an incident wavelength of 10 μm. In the simulation, the dielectric constant of graphene is derived from its conductivity σ_g with: $\varepsilon_g = 1 + i\sigma_g/\varepsilon_0\omega_0 t$, where t is the thickness of graphene which is set to be a non-physical value of 1nm. Such a definition of the dielectric constant makes sure that the simulation result is independent on t. The conductivity of graphene is described with the Drude model [16]:

#217429 - $15.00 USD Received 21 Jul 2014; revised 17 Aug 2014; accepted 23 Aug 2014; published 11 Sep 2014

$$\sigma_g = \frac{e^2 E_f}{\pi \hbar^2} \frac{i}{\omega_0 + i\tau^{-1}} \tag{2}$$

in which E_f and τ are the Fermi energy and relaxation time, and are set to be 0.64eV and 0.64ps respectively in the simulation.

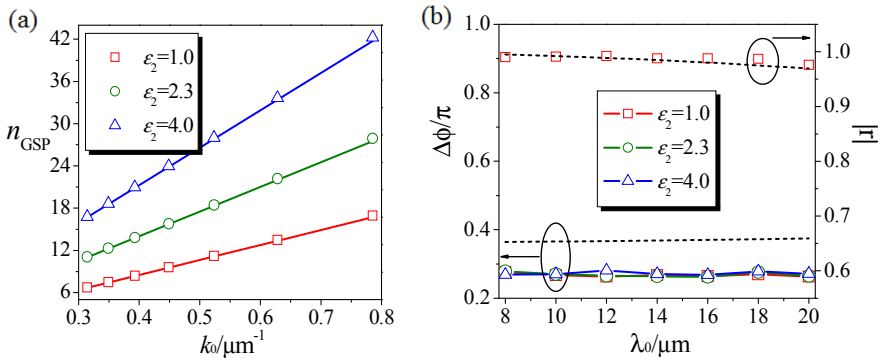

Fig. 2. (a) The effective mode indices of graphene plasmon plotting against the incident wavenumber at various substrate permittivities ε_2. The open scatterers are the values obtained from the self-interference patterns and the solid lines are the theoretical curves. ε_1 is set to be 1 in all of the simulations and calculations. (b) The reflection amplitudes and phases at the mid-infrared region extracted from the self-interference patterns (open scatterers), along with the spectral curves from an analytical estimation (dashed lines). The amplitude is shown only for the case of $\varepsilon_1 = \varepsilon_2 = 1$.

In Fig. 1(b) where no boundary exists, the SP wave launched by the dipole source propagates freely along graphene, with its energy gradually damped because of the intrinsic Ohmic losses of SP mode, rendering a cone-shaped contour pattern. Once there is a boundary, the SP wave will be partially reflected back by the graphene edge and interfere with the incident SP wave, giving rise to an interference pattern as shown in Fig. 1(c). The locations of the interference fringes are determined solely by the phase pickup of SP at the boundary. Assuming that the boundary of graphene locates at $x = 0$, the electric field can mathematically be expressed as:

$$E_z = E_{z,i} + E_{z,r} = E_0 e^{-i\beta(x-x0)} e^{-k_z z} + |r| e^{i\Delta\varphi} E_0 e^{i\beta(x+x_0)} e^{-k_z z} \tag{3}$$

By fitting the electric field from FDTD [Fig. 1(c)] with Eq. (3), the phase pickup of graphene plasmon together with the reflection magnitude and wave-vector can be obtained.

The open scatterers in Fig. 2(a) show the wavelength dependence of the effective mode index (n_{GSP}) of graphene surface plasmon at various substrate permittivities (ε_2). The effective index defined as β/k_0 (k_0 the incident wave-vector) describes the spatial confinement of an SP mode. Theoretically, it can be obtained by substituting Eq. (2) into Eq. (1):

$$n_{GSP} = \frac{\beta_{real}}{k_0} = \frac{\varepsilon_0(\varepsilon_1 + \varepsilon_2)}{2} \cdot \frac{2\pi\hbar^2 c^2}{e^2 E_f} \cdot k_0 \tag{4}$$

The dispersion curves are shown in Fig. 2(a) with the solid lines, in-line well with the results extracted from the interference pattern. This validates the effectiveness of our graphene plasmon modeling with FDTD. The mode index shows a positive relationship with the refractive index of environments surrounding graphene. This is reasonable as an optically dense medium is more effective on confining the electromagnetic field. The magnitude of n_{GSP} is typically on the order of 10^1. This is much higher than that of noble metal plasmon which is close to 1.

#217429 - $15.00 USD Received 21 Jul 2014; revised 17 Aug 2014; accepted 23 Aug 2014; published 11 Sep 2014

The high mode index will intuitively give rise to a high degree of reflection of SPs when hitting a boundary. Figure 2(b) (open scatterers) gives the amplitude and phase of the reflection coefficients extracted from the interference patterns. As inferred, the amplitudes are more than 97% at the full mid-infrared spectrum region. The phases acquired upon reflection range from 0.26π to 0.28π at the same region and more interestingly, is likely insensitive on ε_2 and hence on the effective dielectric constant of the environment ($(\varepsilon_1 + \varepsilon_2)/2$) as ε_1 and ε_2 play an identical role on graphene plasmons. The spectral response of the reflection coefficient is unfortunately not clearly indicated by the FDTD modeling because of: 1) the small variation of coefficient at the spectrum region considered and 2) the variant meshing sizes at different wavelengths which may cause fluctuation of the modelling results.

To uncover the spectral trend, we carry out an analytical estimation based on the idea proposed in [38]. Briefly, the electromagnetic fields at the graphene half space ($x>0$) are expressed as the summation of incident and reflected SP waves while those scattered into the free half space ($x<0$) are formulated with the angular spectrum representation. The reflection coefficient can be obtained by matching the tangential magnetic (H_y) and perpendicular electric field (E_z) at the pseudo boundary plane ($x = 0$), which has a Fresnel-like reflection coefficient under normal incidence:

$$r = \frac{n'-1}{n'+1} \tag{5}$$

where

$$n' = \frac{\pi}{2}\left[\int_{-\infty}^{\infty} \frac{1}{\sqrt{1-u^2}} \left(\frac{u \cdot n_{GSP}}{u^2 + n_{GSP}^2}\right)^2 du\right]^{-1} \tag{6}$$

$u = k_z/k_0$ is the normalized perpendicular wave-vector. From Eq. (5), the imaginary part of n' gives rise to a non-zero reflection phase and Eq. (6) clearly indicates that this imaginary part arises from the $u>1$ components, i.e., the electromagnetic evanescent components scattered into the free half space. For simplicity, we consider only the case when $\varepsilon_1 = \varepsilon_2 = 1$. The calculated reflection amplitudes and phases are shown in Fig. 2(b) with the dashed lines. In consistent with the above analysis, the magnitude of reflection decreases monotonically with respect to the incident wavelength because of the reduced mode index. The reflection phase, on the contrary, shows a monotonic increase. However, the rate is rather low (0.364π-0.374π at the spectrum region considered) and hence it can approximately be treated as a constant at the mid-infrared region. It is noted that the magnitude of phase pickup calculated from Eq. (5) deviates from the ones from FDTD modeling. This may result from the neglect of the local modes confined at the graphene edge except for the propagating graphene plasmons [42]. However, we conclude that such neglect will not give a significant change on the spectral trend of the reflection coefficient.

#217429 - $15.00 USD Received 21 Jul 2014; revised 17 Aug 2014; accepted 23 Aug 2014; published 11 Sep 2014

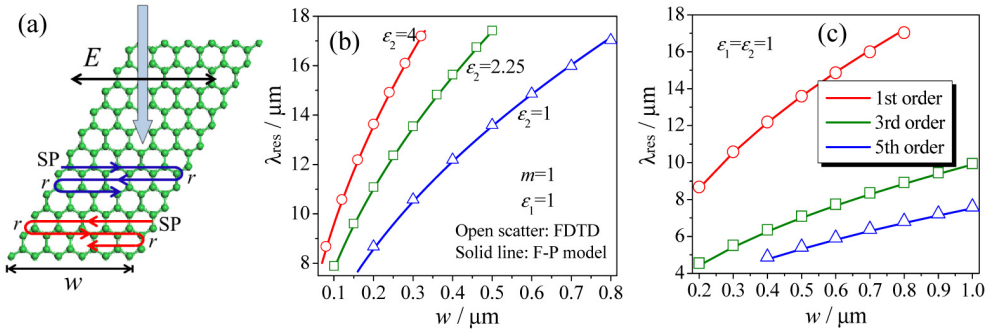

Fig. 3. Plasmonic resonance of an isolated graphene nano-ribbon. (a) Schematic diagram illustrating the excitation of plasmon modes on an isolated graphene ribbon with normal incidence. (b) Resonance wavelengths of the fundamental modes of isolated graphene ribbons from FDTD (open scatterers) as compared with the results from F-P model, assuming a reflection phase of 0.27π (solid lines). (c) Resonance wavelengths of the higher order plasmon modes and the comparison.

3. Fabry-Perot resonances of graphene nano-ribbons

With the reflection coefficient, a plasmonic F-P model can be formulated to forecast the resonances of graphene nano-ribbons. We first consider the case of an isolated graphene ribbon. Assuming that a laser beam of wavelength λ_0 is incident normally on to graphene, with light polarization across the ribbon [Fig. 3(a)], SPs will be launched at both of its edges and undergo multiple round trips within the ribbon because of the edge reflection. Eventually, the electric field right above graphene can be expressed as:

$$E_z = E_z^{left} + E_z^{right} = \frac{2iE_0 e^{i\beta w/2}\sin\beta x}{1+|r|\cdot e^{i(\Delta\varphi+\beta w)}} \tag{7}$$

where E_0 denotes the starting field amplitude of SPs, which is related to the light-to-SP coupling efficiency, E_z^{left} and E_z^{right} represent the superposition of SP fields launched from the left-side (blue) and right-side (red) edges, respectively. The denominator in Eq. (7) should be a pure real number in order for the electric field to reach its maximum value (resonance). This requires that:

$$\beta_r \cdot w + \Delta\varphi = m\pi \quad m = 1, 2, 3, \ldots \tag{8}$$

the well-known F-P resonance equation. Here, β_r is the real part of SP wave-vector, w the ribbon width and $\Delta\varphi$ the phase pickup upon edge reflection. After substituting the expression of β_r, the scaling law of graphene plasmons at the ribbon configuration can be obtained:

$$\omega_0 = \sqrt{\frac{e^2 E_f}{\varepsilon_0 \hbar^2 w}\cdot\frac{m-\Delta\varphi'}{(\varepsilon_1+\varepsilon_2)}} \tag{9}$$

in which $\Delta\varphi' = \Delta\varphi/\pi$ is the normalized phase.

Figure 3(b) shows the resonance curves for the fundamental modes (m = 1) of an isolated graphene ribbon predicted with the plasmonic F-P model [Eq. (9)], together with the results obtained with FDTD method. The phase pickup of 0.27π (the averaged phase as obtained in Fig. 2(b) with FDTD) was employed for the calculation. The excellent agreement between the results from FDTD and F-P model are clearly illustrated. For the fundamental mode, the resonant condition from Eq. (8) is $w/\lambda_{sp} = (1-\Delta\varphi')/2 \approx 0.37$, well explaining the experimental results in [20]. We further simulated the high-order plasmon modes with FDTD and compared with the F-P model. The results are shown in Fig. 3(c), presenting good agreement.

#217429 - $15.00 USD Received 21 Jul 2014; revised 17 Aug 2014; accepted 23 Aug 2014; published 11 Sep 2014

These unambiguously verify the effectiveness of the F-P model for predicting the resonance of an isolated graphene ribbon. In Fig. 3(c) we provide the results only for the odd plasmon modes as the even modes cannot be excited with the normal incidence excitation configuration. This will be explained in detail in the following part.

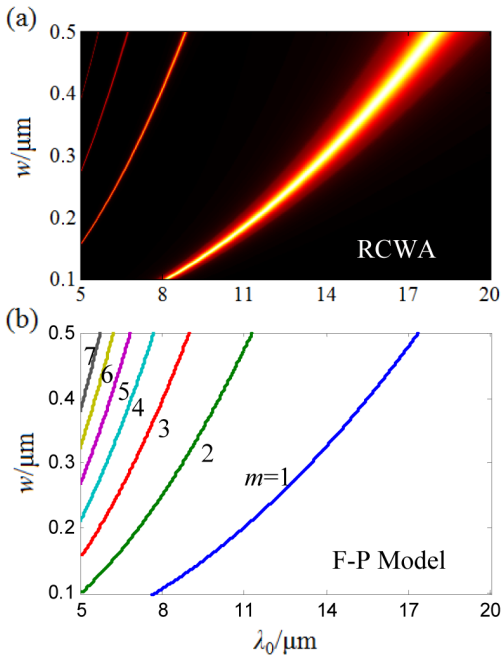

Fig. 4. (a) The absorption contour pattern of periodic ribbon structures at the mid-infrared region, with ribbon width ranging from 100 nm to 500 nm. The width-to-period ratio is fixed at 1/2 in the simulation. (b) Resonance curves as calculated with the F-P formula at the same spectrum region and width range as in (a), assuming a constant reflection phase of 0.27π.

We then consider a periodic ribbon structure whose resonance picture can easily be obtained by using the rigorous coupled-wave analysis (RCWA) [43]. In our simulations, the ribbon width-to-period ratio is fixed at 1/2. The absorption contour map obtained with RCWA and the resonance curves calculated with Eq. (9) are shown in Figs. 4(a) and 4(b), respectively. Figure 4 clearly indicates that only the odd modes are excited (i.e. m = 1,3,5,…), while the even modes (m = 2,4,6…) disappear at the absorption map. This is owing to the fact that, at each of the ribbons, SPs are launched from both of its edges and are initially out of phase. As a result, although the superposition of SP waves for each of the sub-branches (red/blue branch) is constructive when m is even, the interference between the two subsets is exactly destructive and hence no resonance occurs. This can also be read from Eq. (7), in which the denominator equals to $1 + |r|\cdot\exp(-\beta_i w)$ (β_i the imaginary part of β) when m is even, which indeed gives rise to a minimum value of electric field. Nevertheless, the even plasmon modes can be excited as long as the SPs are launched in phase from the two edges. Under this circumstance, the electric field would be expressed as

$$E_z = E_z^{left} + E_z^{right} = \frac{2E_0 e^{i\beta w/2}\cos\beta x}{1 - r\cdot e^{i(\Delta\varphi+\beta w)}} \tag{10}$$

which reaches maxima only when m is an even number. In practice, this can be realized by placing a near-field SPs emitter (such as molecules or quantum dots) right above the center of graphene, with polarization perpendicular to the ribbon, as demonstrated in [22]. In a word,

#217429 - $15.00 USD Received 21 Jul 2014; revised 17 Aug 2014; accepted 23 Aug 2014; published 11 Sep 2014

both the even and odd plasmon modes are the eigen-modes of graphene ribbons while they require different configurations to excite them.

Figure 4 also indicates that the resonance wavelengths from the absorption map show red shift with respect to the ones calculated from the F-P model. This should attribute to the electromagnetic coupling between the graphene ribbons and we assume that such interaction will induce a change on the reflection phase.

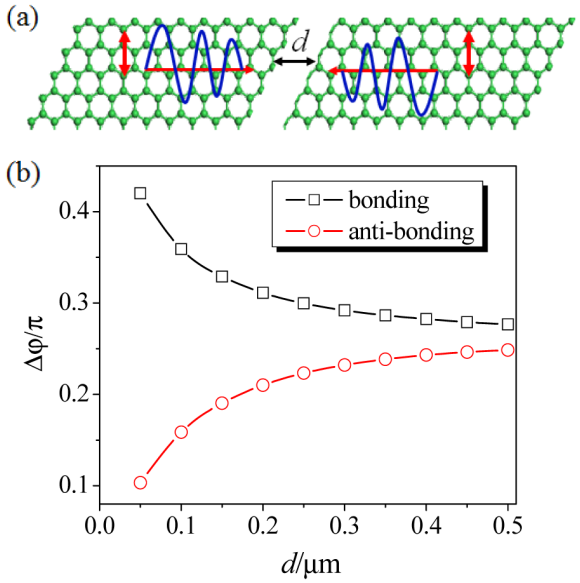

Fig. 5. (a) Schematic diagram illustrating the modeling of edge-reflection phase under a pair of neighboring coplanar graphene sheets with separation of *d*. A pair of line dipole sources located symmetrically with respect to the slit center is employed to launch the SPs separately at each of graphene sheets. (b) The splitting of phase results from the coupling between the two graphene sheets.

3. Fabry-Perot resonances of graphene nano-ribbons

To verify our assumption, we further study the phase pickup upon reflection in the case of a pair of neighboring coplanar graphene sheets with separation *d*, as illustrated in Fig. 5(a). A pair of line dipole sources right above graphene and located symmetrically with respect to the slit center is employed to launch the SPs independently at each of the graphene sheets. Their coupling schemes (bonding/anti-bonding) thus can easily be tuned by changing the phase of the two dipole sources (in-phase/out-of-phase).

Figure 5(b) gives the magnitude of phase pickup under both the bonding and anti-bonding coupling schemes, clearly showing a phase-splitting. The bonding coupling between the two graphene sheets lifts up the phase, with an increasing rate at the smaller separation. This will give rise to a red shift of the resonance wavelength as indicated with Eq. (9). The anti-bonding coupling, in contrast, drags down the phase and would result in a blue shift of the resonance wavelength. For a periodic ribbon structure, only the bonding coupling mode survives as the anti-bonding mode displays a zero net dipole moment, hence leading to a red-shift of resonance wavelength with respect to an isolated graphene ribbon. The anti-bonding mode, however, does exist in terms of a wave-guiding mode propagating along the graphene ribbon. The dispersion diagram presents an energy-splitting for a pair of coplanar ribbons as demonstrated in [23], which could potentially be explained with the phase-splitting induced by the inter-ribbon interaction.

#217429 - $15.00 USD Received 21 Jul 2014; revised 17 Aug 2014; accepted 23 Aug 2014; published 11 Sep 2014

5. Conclusion

To summarize, the reflection magnitude and phase of graphene surface plasmons at the boundary was studied. At the mid-infrared spectrum region, graphene plasmons are nearly totally reflected because of their high mode indices, together with an approximately constant phase jump of 0.27π. With the reflection coefficient, a plasmonic Fabry-Perot model is formulated that can predict well the resonance wavelengths of isolated graphene nano-ribbons. Applying the same approach, we further illustrate the phase-splitting when two graphene sheets couple with each other. Their bonding coupling will lift up the reflection phase, leading to a red-shift of the resonance wavelength of a periodic ribbon structure. The splitting of reflection phase could also potentially interpret the energy splitting of the plasmonic wave-guiding modes at a pair of coplanar ribbons. The work in this article presents a physical insight of the resonances of graphene nano-structures and would be helpful for designing and engineering the graphene resonators and waveguides as well as their associated applications.

Acknowledgment

This work was partially supported by the Minister of Education (MOE) Singapore under the grant no. 35/12 and the National Natural Science Foundation of China under Grant Nos. 61036013, 61138003.

#217429 - $15.00 USD Received 21 Jul 2014; revised 17 Aug 2014; accepted 23 Aug 2014; published 11 Sep 2014